Directional and Polarized Emission from Nanowire Arrays

Dick van Dam,*[,†] Diego R. Abujetas,[‡] Ramón Paniagua-Domínguez,[‡] José A. Sánchez-Gil,[‡] Erik P. A. M. Bakkers,[†,§] Jos E. M. Haverkort,[†] and Jaime Gómez Rivas*[,†,∥]

[†]Department of Applied Physics, Eindhoven University of Technology, P.O. Box 513, 5600 MB Eindhoven, The Netherlands

[‡]Instituto de Estructura de la Materia (IEM-CSIC), Consejo Superior de Investigaciones Científicas, Serrano 121, 28006, Madrid, Spain

[§]Kavli Institute of Nanoscience, Quantum Transport, Delft University of Technology, 2600 GA Delft, The Netherlands

[∥]FOM Institute AMOLF, c/o Philips Research, High-Tech Campus 4, 5656 AE Eindhoven, The Netherlands

S *Supporting Information*

ABSTRACT: Lighting applications require directional and polarization control of the emitted light, which is currently achieved by bulky optical components such as lenses, parabolic mirrors, and polarizers. Ideally, this control would be achieved without any external optics, but at the nanoscale, during the generation of light. Semiconductor nanowires are promising candidates for lighting devices due to their efficient light outcoupling and synthesis flexibility. In this work, we demonstrate a precise control of both the directionality and the polarization of the nanowire array emission by changing the nanowire diameter. We change the angular emission pattern from a large-angle doughnut shape to a narrow-angle beaming along the nanowire axis. In addition, we tune the polarization from unpolarized to either p- or s-polarized. Both the far-field emission pattern and its polarization are controlled by the number and type of guided or leaky modes supported by the nanowire, which are determined by the nanowire diameter.

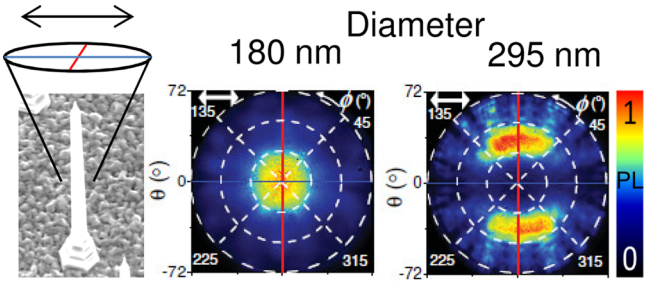

KEYWORDS: *Nanowires, Fourier microscopy, polarization, emission, directionality*

Controlling the polarization and directionality of the emission of nanosized light sources is of great importance in the engineering of light-emitting diodes (LEDs),[1−4] nanolasers,[5,6] and applications in quantum optics such as single photon sources.[7−10] The bottom-up growth of semiconductor nanowires (NWs) allows a large design flexibility in parameters such as nanowire position, size, interwire distance, and crystallographic orientation. This makes nanowires interesting candidates for the design of nanosized light emitters and detectors.[11]

Wide-range control over the direction of the nanowire emission has not yet been reported. Previous studies have indicated the two main mechanisms that affect the nanowire emission directionality.[12−14] Recently, the directional emission of thin InP nanowires has been explained by coupling to leaky waveguide modes in the nanowire.[15] These modes modify the direction of the nanowire emission, causing an antenna-like behavior.[7,15,16] Identification of the relevant guided/leaky nanowire modes is important in tuning the direction of the far field emission.[17] The second mechanism that was associated with the emission directionality of NW arrays is the coupling of the emission to resonances in periodic arrays of nanowires, which behave as quasi-two-dimensional photonic crystals. The photoluminescence excited in one of the nanowires may couple to Bloch modes supported by the periodic structure and couple out to free space in certain directions. This directional outcoupling has been theoretically[18] and experimentally demonstrated.[14,19] So far, no study—either theoretically or experimentally—of the interplay of both described mechanisms has been reported.

In addition to directionality, control over the emission polarization is important for many applications, such as solid-state lighting, sensing, and optical communication. Thin nanowires have the ability to emit strongly polarized light,[20,21] which is a useful property for displays and sensing[2] but may hinder the application in quantum optics.[22] The nanowire polarization anisotropy has been first explained in the electrostatic limit by the elongated shape of the nanowires and the high refractive index contrast with the environment,[20] and it has later been described in terms of coupling to Mie resonances.[22] On top of that, the selection rules of the band structure of the emitting material also affect the polarization.[21] However, it is unknown how the polarization of the nanowire emission depends on the diameter, taking into account both waveguide modes and selection rules.

In this Letter we discuss the polarized and directional emission properties of semiconductor nanowire arrays, which

were analyzed through Fourier microscopy. We demonstrate that the nanowire diameter is the essential parameter, providing control over the directionality of the emission, and show that similar far-field emission patterns can have totally different polarized emission. This behavior is explained by the coupling of the emission to different waveguide modes confined to the nanowire. In addition, the emission pattern is modulated by the periodic array.

Our sample consists of arrays of indium phosphide (InP) nanowires with a period ranging from 0.8 to 5 μm. A combination of axial vapor−liquid−solid (VLS), radial vapor−solid (VS) growth, and the varying period led to different nanowire diameters for the different arrays. The growth is described in more detail in the Methods section. A scanning electron micrograph of the sample can be found in Figure 1a,b,

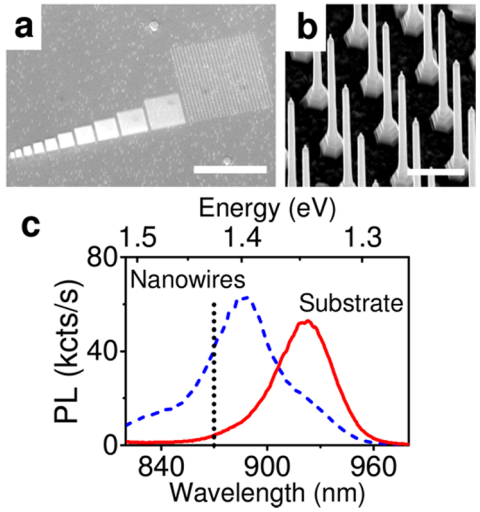

Figure 1. Nanowire sample information. (a) Scanning electron micrograph (SEM) of the sample with different nanowire arrays and (b) a close-up of one of the nanowire arrays. The images were taken at 30° glancing angle; the scale bars are 100 and 2 μm, respectively. (c) Photoluminescence (PL) emission spectrum of nanowires (blue, dashed line) and the underlying substrate (red, solid line). The black dotted line indicates the transmittance maximum of the band-pass filter used for the Fourier emission measurements.

and a typical photoluminescence spectrum of nanowires and substrate is shown in Figure 1c. The mixed wurtzite−zinc blende crystal structure of the nanowires gives rise to blue-shifted emission compared to the zinc blende emission from the substrate. The emission patterns of the nanowires were obtained by Fourier microscopy as described in detail in the Supporting Information, section 1. In a Fourier microscope the back focal plane of the objective is imaged in order to obtain the parallel (in-plane) components of the wave vectors of the far-field emission. These wave vectors can be converted into emission angles as explained elsewhere.[23] The Fourier images were collected in a CCD camera with a band-pass filter with a transmission maximum at 870 nm (dotted black line in Figure 1c) and a bandwidth of 10 nm. For all nanowire arrays, a small fraction of the emission transmitted through the band-pass filter stems from the substrate, as can be appreciated from Figure 1c. This fraction is lower than 25% for all the arrays (typically 10%) and depends on the amount of absorption of the excitation beam in the nanowires. The small fraction of emission from the substrate causes a Lambertian-like background in the Fourier images, without qualitatively affecting them.

First, we focus on single-nanowire effects in the emission patterns. We will discuss the interaction with the surrounding array later. The excitation beam has a diameter of about 1 μm on the sample, therefore exciting only one nanowire in all arrays. Figures 2a−c show polar plots of the measured unpolarized far-field emission patterns of nanowires with three different diameters d (100 ± 10, 180 ± 6, and 295 ± 13 nm, referred to as "thin", "intermediate", and "thick"). In this emission pattern series, we observe a remarkable change from doughnut-shaped emission (Figure 2a) to narrow-angle beaming at small angles with respect to the nanowire's axis (Figure 2b). Interestingly, the emission pattern from the thickest nanowires again reveal a doughnut-shaped far-field emission (Figure 2c). These images illustrate that it is possible to totally change the direction of the emission by tailoring the nanowire diameter.

For further insight into the origin of this remarkable phenomenon, we have measured the polarized directional emission patterns of the nanowires by placing a polarizer in front of the Fourier camera. The polarized emission patterns are shown in Figures 2d−f. In this configuration, the emission recorded along the polarizer's transmission axis (horizontal direction) is purely p-polarized, whereas the emission recorded along the orthogonal axis (vertical direction) is purely s-polarized.[15] A full description of the polarization-dependent collection is provided in the Supporting Information (Figure S2). We experimentally observe that the light is almost entirely p-polarized for small nanowire diameters. On the contrary, we observe that the thick nanowires emit strongly s-polarized light, while the polarized emission pattern of the intermediate nanowire is unpolarized. To understand the origin of this variation, we investigate the role of the waveguide modes supported by the nanowire geometry.

The dispersion of the available waveguide modes within a nanowire can be calculated from Maxwell's equations, applied to an infinite cylinder (as explained in the Supporting Information, section 2), and is shown in Figure 3a. Note that the diameters expressed in the dispersion diagram are calculated for a circular cross section, while our nanowires have a hexagonal cross section. It has been shown that the modes for a hexagonal nanowire cross section are equivalent to modes for a circular nanowire cross section with a slightly lower diameter.[24] Therefore, we choose the "equivalent circular diameters" to be 90, 165, and 275 nm, respectively. The dispersion curves are labeled as transverse magnetic (TM), transverse electric (TE), and magnetoelectric (HE) modes. The light cones of air and InP are expressed using the white and dashed areas in Figure 3a. Waveguide modes are "leaky" if their dispersion curve is in the air light cone. In this case, the mode radiates (leaks) into the surrounding medium (air). If the dispersion curve is in the InP light cone, the mode is guided by the nanowire. From the dispersion relation we obtain the propagation constant k_z for each mode, at the diameter of interest. Using the k_z's, we can calculate the far-field patterns of the available waveguide modes by the 1D current model, described in ref 17. In this model the nanowire emission is fully determined by a line current $\mathbf{I}(z)$ produced by a point dipole at position z_0 exciting a leaky/guided mode.[17] The equations used in the model are listed in the Supporting Information, section 3.

We compare the calculated emission patterns to the measurements in order to determine which mode has the

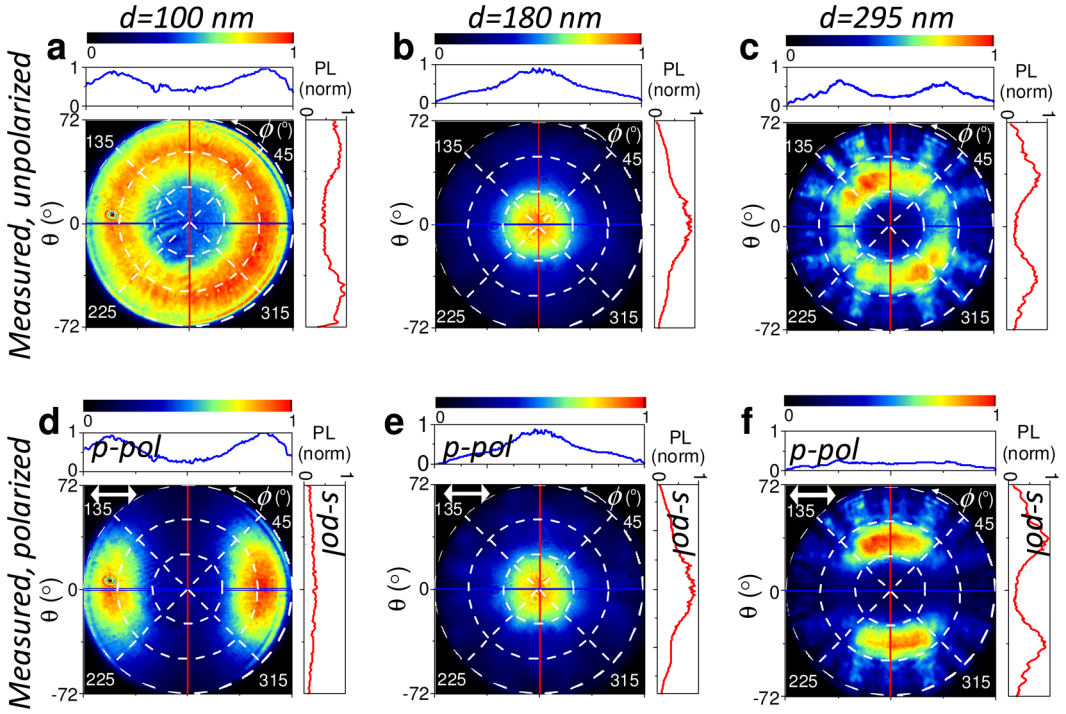

Figure 2. Fourier images of emission. All intensities are normalized to their maximum value. (a–c) Unpolarized Fourier emission patterns for three different nanowire diameters *d*: 100, 180, and 295 nm, respectively. The color indicates the normalized PL intensity. Cuts through the center are displayed at the top and right side of each color plot. (d–f) Same as (a–c), but the emission recorded through a linear polarizer oriented along the white double arrow in each plot. The p-polarized emission is recorded along the horizontal axis (blue profile, p-pol) and s-polarized emission along the vertical axis (red, s-pol).

dominant contribution to the emission. The calculated polarized emission patterns (for the dominant modes) are shown in Figures 3b–d; the other patterns are displayed in the Supporting Information. These patterns can be directly compared to the measured polarized patterns (Figures 2d–f). The color plots and polarized profiles (cuts at top and right side of each color plot) show a very similar shape. From the good qualitative correspondence between experimental and modeled polarized patterns, we conclude that the differently polarized patterns are caused by different waveguide modes. For the thin nanowire the emission is determined by the leaky TM_{01} mode and not by the weakly guided HE_{11} mode. This counterintuitive result is caused by the larger electric field intensity of the leaky TM_{01} mode inside the nanowire compared to that of the fundamental HE_{11} mode, whose electric field is mainly present in the surrounding medium (Supporting Information Figure S4). Therefore, the emission from a source located in the nanowire preferentially couples to the TM_{01} mode.[15] For the intermediate nanowire diameter the emission is given by the guided HE_{11} mode. In this case, the electric field of the HE_{11} mode is better confined inside the nanowire. Finally, for the thickest nanowire, the emission couples preferentially to the guided TE_{01} mode. The main differences between the measurements and the calculation are at the background of the measurements, which is due to the contribution of the substrate to the emission, and the broader peaks in the measurements due to inhomogeneities in the sample. In the calculations for the thickest nanowires (Figure 3d) we observe emission at large emission angles ($\theta > 50°$), which is not visible in the measurement (Figure 2f). This absence of large-angle emission is explained by scattering of the nanowire emission due to the surrounding array. The interaction between the nanowire and the surrounding array will be discussed later.

We have also investigated whether the responsible waveguide modes can be excited from the luminescence in the nanowire. Therefore, we have performed the finite-element method (FEM) simulations based on emitting dipoles inside the NW (shown in the Supporting Information, section 3), which indeed confirm the coupling of the emission to the aforementioned waveguide modes. We conclude that by tailoring the waveguide modes, we are able to drastically change the angular distribution and polarization of the far-field emission.

To investigate the polarization-dependent emission in more depth, we have determined the polarization anisotropy of the emission as a function of the nanowire diameter. The polarization anisotropy ρ is generally defined as $\rho = (I_{\parallel} - I_{\perp})/(I_{\parallel} + I_{\perp})$, where $I_{\parallel}$ and $I_{\perp}$ are the parallel and perpendicular polarized emission intensities with respect to the nanowire axis.[20,25] In our angle-dependent configuration, $I_{\parallel} = I_p \sin\theta$ and $I_{\perp} = I_s$, where θ is the emission angle with respect to the nanowire axis. The polarized emission intensities I_p and I_s are obtained by integrating the polarized emission patterns along the horizontal and vertical axes ($\phi = 0°–180°$ and $\phi = 90°–270°$), respectively.

In Figure 4, we show the polarization anisotropy of the measured nanowire emission as a function of the nanowire diameter (black spheres). These data are the polarization anisotropies integrated over all angles θ captured by the microscope objective, i.e., from 0° to 72°. We observe a gradual decrease in ρ, being a transition from parallel to perpendicular polarized emission, when increasing the diameter. To investigate the dependence of the polarization anisotropy on

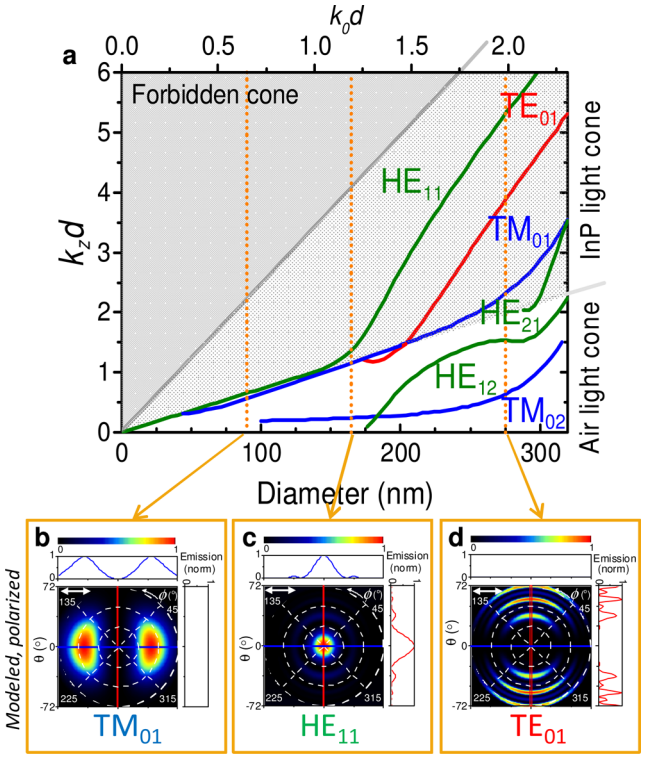

Figure 3. Waveguide modes account for direction and polarization of the emission. (a) Dispersion relation of leaky and guided modes for an infinitely long cylinder with diameter d, expressed as (real part of) wavenumber k_z against size parameter k_0d. At the bottom horizontal axis the diameter is shown for a cylinder with n = 3.43 (InP) at 870 nm. Vertical dotted lines indicate the three diameters that we have further investigated. (b–d) Modeled emission patterns that correspond to the patterns in Figures 2d–f, calculated using the 1D current model. The specific mode for which the pattern is calculated is indicated below each image.

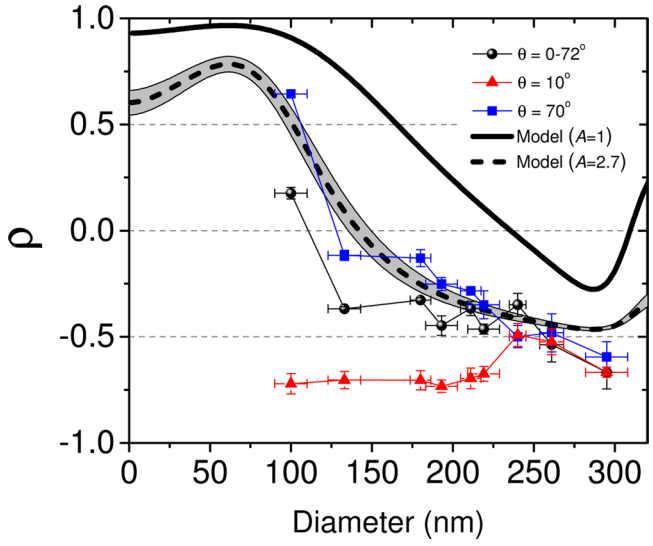

Figure 4. Role of dielectric contrast and viewing angle in polarization. Data points show the measured polarization anisotropy as a function of the nanowire diameter, for emission angles integrated over 0–72° (black spheres) or at 10° (blue squares) and 70° (red triangles). The data points are connected as a guide to the eye. Error bars denote the statistical variance in diameter (determined by SEM imaging) and polarization anisotropy. The solid line is the calculated polarization anisotropy following the model of Ruda and Shik, for dipole anisotropy ratio A = 1. The dashed line is the model with the fitted value A = 2.7. The gray shaded area indicates the standard error of the fitted curve.

the emission angle θ, we determine ρ for a small (10°, red triangles) and a large angle (70°, blue squares). We observe a large difference in polarization anisotropies between the different emission angles. At small θ, a small ρ is found because of the low $I_{\parallel}$ in this direction. There is no strong change in ρ depending on the diameter, except for the diameters larger than 200 nm, where coupling to the transverse (polarized) guided modes (TM_{01} and TE_{01}) is possible. At large θ, a clear decrease of ρ is visible. It is important to mention that previous reports of the polarization anisotropy of the emission of single nanowires were based on measurements done by collecting the emission with large-NA objectives.[20−22,26,27] The strong angle dependence of the polarization anisotropy of the nanowires indicates that it is important to consider the NA of the objective when analyzing this polarized emission. Clearly, the choice of NA (and therefore maximum captured emission angle θ_{max}) affects the measured value of polarization anisotropy. Fourier microscopy allows measuring the angle-dependent polarization anisotropy, thus taking into account this peculiar phenomenon.

The decreasing trend of ρ for increasing diameter at θ = 70° is explained by a model for the polarization anisotropy as a function of the normalized frequency $\omega a/c$, which was introduced by Ruda and Shik.[25] This model considers an isotropically oriented emitting dipole embedded in an infinitely long nanowire and describes the emission at an angle θ = 90° with respect to the nanowire axis. In this model (equations are given in the Supporting Information, section 4), the polarization anisotropy of the emission is explained by the dielectric contrast between the nanowire (which in our case has refractive index n = 3.43 and radius a) and the surrounding medium (n = 1), causing a suppression of the perpendicularly polarized electric field inside thin nanowires. The explanation of the polarization anisotropy of nanowires in terms of the dielectric contrast has been identified to Mie resonances and leaky modes, showing that these descriptions are equivalent to one another.[15,22,23] The values of ρ calculated with this model, for InP at 870 nm, are plotted in Figure 4 as a solid line. The suppression of the perpendicular electric field causes a strong polarization parallel to the nanowire, i.e., $\rho \approx 1$, for the thin nanowires, $\omega a/c \ll 1$. For larger values of $\omega a/c$, ρ decreases until a local minimum around d = 280 nm and increases again.

At small angles (θ = 10°), the Ruda and Shik model fails in describing the measurements. As mentioned above, this model only describes the emission at large angles (θ = 90°), where there is no contribution from guided modes. At large angles (θ = 70°) the decreasing trend of ρ from the model is followed by the measurements, indicating that in this condition the dielectric contrast between the nanowire and the surrounding air is dominating the polarization anisotropy. However, there is a vertical offset between measurement and model. To investigate this offset, we look in more detail to the differences between experiment and model. The effect of the difference in θ between measurement and model (70° vs 90° is negligible, since sin 70° ≈ sin 90°. Therefore, the explanation for the difference should be found in an anisotropic internal emission of the differently oriented dipoles. The model contains the intrinsic emitting dipole strengths d_{0x}, d_{0y}, and d_{0z} for dipoles oriented perpendicular and parallel to the nanowire axis. The

ratio $A \equiv d_{0x}/d_{0z} = d_{0y}/d_{0z}$ is set to 1 (isotropic internal emission) in the calculation represented by the black solid line in Figure 4. Fitting this parameter A to the measured large-angle polarization anisotropy gives a value of $A = 2.7 \pm 0.3$. The fit is added to Figure 4 (dashed line). This value of A indicates a larger emission strength of the perpendicular dipole, which could be explained by the selection rules of the wurtzite crystal phase of the nanowire. These selection rules affect the dipole strengths of the emitting transitions. In zinc blende crystal phase both parallel and perpendicular polarizations are allowed. However, in wurtzite crystal phase only the perpendicular polarization is allowed.[28,29] Our nanowires are predominantly wurtzite (as can be concluded from the PL spectrum in Figure 1c), so emission from dipoles polarized perpendicular to the nanowire will dominate. Using the band-pass filter shown in Figure 1c, we select mainly the emission of the wurtzite InP band gap, which results in an increase of A and a decrease of the measured value of ρ.

In order to describe the interplay between the waveguide modes in the nanowire and the Bloch modes in the periodic array, we show the directional emission of a nanowire array with a pronounced square symmetry, imposed by the 2D nanowire array (Figure 5a). This array has a nanowire diameter

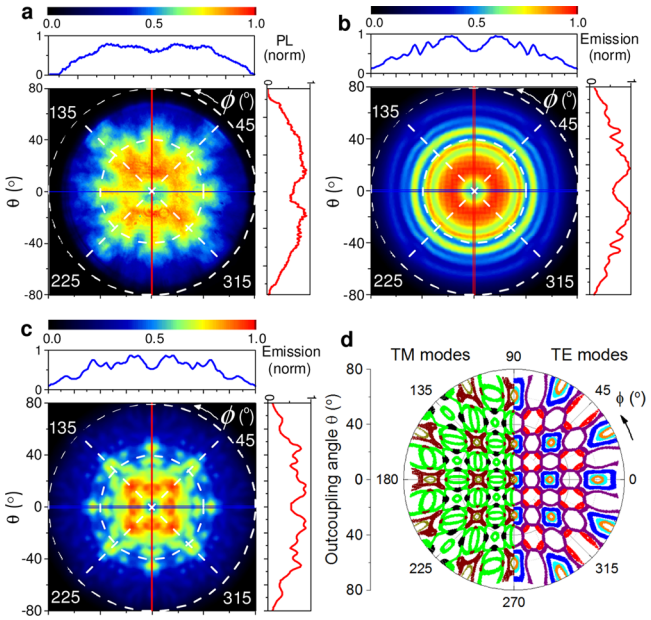

Figure 5. Effect of surrounding array on directional emission pattern. The intensities are normalized to their maximum value. (a) Fourier emission pattern of a nanowire array with period $p = 2$ μm and nanowire diameter $D = 219$ nm. Intensity profiles through horizontal and vertical axes are shown at top and right side. (b) FDTD simulated far-field pattern of three orthogonal dipoles in the center of a single nanowire, without surrounding array. (c) FDTD simulated far-field pattern for a nanowire inside an array with $p = 2$ μm. (d) Outcoupling angles of Bloch modes for the same array; different colors represent different eigenmodes in a 2D photonic crystal. The left side shows TM modes and the right side TE modes.

$D = 219 \pm 9$ nm and an array period $p = 2$ μm. To model the far-field emission pattern of nanowires placed in an array, we have performed numerical electromagnetic simulations of the nanowires under study, using the finite-difference time-domain (FDTD) method. This allows us to quantify the relative contributions of waveguide modes and Bloch modes to the far-field emission pattern. First, we obtain the emission pattern from a point dipole embedded in a single nanowire with dimensions equal to the measured nanowire. For simplicity, the dipole is located in the center of the nanowire. As is shown below, this gives a good agreement with the measurements. Varying the position of the dipole over the nanowire changes the coupling efficiency to the different guided modes. This is discussed in detail elsewhere.[17,30] A monitor on top of the nanowire records the fields generated by the simulation, and a near-to-far-field transformation is used to derive the far-field pattern. Further details of the simulations can be found in the Supporting Information, section 3. The simulated far-field emission pattern of the single nanowire is depicted in Figure 5b. The directional emission measurement and corresponding simulation show a similar emission pattern: a local minimum for $\theta = 0°$ and a doughnut shape with a maximum at about $\theta = 20°$. The measurement however shows a pronounced square symmetry, deforming the doughnut shape, which is absent in the simulation.

To determine the contribution of the array to this emission pattern, we have also calculated the far-field emission patterns of emitting dipoles embedded in the central nanowire of a 7 × 7 nanowire array, which is shown in Figure 5c. The general pattern of the emission is preserved: a minimum for $\theta = 0°$ and a maximum at about $\theta = 20°$. This can be clearly seen at the profile cuts in Figure 5. However, the array modulates the emission pattern, imposing the square symmetry that is seen in the measurement.

For further insight into the role of the array in the emission, we envision the nanowire array as a 2D-photonic crystal, established by the periodic refractive index modulation, which gives rise to Bloch modes.[14,19,31] The outcoupling angles calculated from the Bloch mode dispersion, corresponding the array of Figure 5a (shown in the Supporting Information, section 5), are shown in Figure 5d. In these calculations, we observe a square-like symmetric angular distribution with a multitude of outcoupling angles for the allowed Bloch modes in the nanowire photonic crystal. We observe that the detailed structure of the emission pattern in Figure 5d resembles the calculated and simulated square-symmetric emission pattern of the nanowire photonic crystal, although our measured profiles show angular broadening due to the finite length of the nanowires and sample inhomogeneities.

From the measurements and simulations of Figure 5, we conclude that the doughnut shape determining the envelope of the emission pattern of the array arises from the modes generated in the individual nanowires, while the square-symmetric features in the array emission patterns are due to coupling of the emission to Bloch modes in the periodic array. However, these modifications are not dominant, as can be appreciated by comparing the cuts of the measurements to the simulations. The emission of the array is thus mainly explained in terms of the emission of individual nanowires as discussed in the previous sections.

A tapering of the nanowire top facet is observed in the SEM images (Figure 1b). Tapering has been related to an enhanced outcoupling efficiency because of the adiabatic expansion of the HE_{11} mode,[8,32,33] for tapering angles smaller than 10°.[32] Since our tapering angle is much larger (approximately 30°), we expect no strong effect, and therefore we did not include the tapering in our modeling. Because we find excellent agreement between simulations and measurements, we conclude that the

mild tapering in our nanowires does not significantly affect the outcoupling of the emission.

In conclusion, we have shown that the directionality and polarization of the emission of nanowires can be precisely tuned by introducing small changes in the nanowire diameter. This remarkable feature is caused by the efficient coupling of the emission to different waveguide modes, which dominate the emission outcoupling and polarization. Tuning the nanowire diameter enables selecting for instance unpolarized beaming or linearly polarized doughnut-shaped emission. This work opens up new possibilities for light-emitting devices and nanosized light sources with predesigned polarization and direction of the emission, without using any external optical element.

Methods. *Sample Description.* The cores of the nanowires are grown using the bottom-up vapor−liquid−solid (VLS) method in a metal−organic vapor-phase epitaxy (MOVPE) reactor. Gold catalyst nanoparticles with diameters of 25 and 50 nm were positioned in square arrays on an InP substrate using electron-beam lithography. The arrays consist of 25 × 25 particles of which the period varies from 0.8 to 5 μm. Halfway the gold-catalyzed core growth, arsenic is added to the system to induce the growth of a InAsP quantum dot of about 10 nm height. (The emission of the quantum dot quenches at room temperature and is not visible in the measurements in this Letter.) After the core growth, the diameter of the nanowire is increased by radial growth of an InP shell at higher temperature. Both the axial and radial growth rates are determined by the period of the array, which causes a different nanowire diameter for the different arrays, ranging from 133 to 295 nm. More details on the growth of the sample can be found elsewhere.[34] The nanowires are grown in mixed wurtzite−zinc blende crystal phase. Because of a difference in electronic band gap between InP in wurtzite and InP in zinc blende phase (1.43 and 1.34 eV, respectively, at room temperature[21,35]), the peaks of substrate emission (around 920 nm) and nanowire emission (around 880−890 nm, due to mixed crystal phase growth) can be easily spectrally distinguished (Figure 1c).

■ ASSOCIATED CONTENT

Supporting Information

Detailed description of the setup and polarization measurements, calculations of the dispersion of waveguide modes and Bloch modes, field profiles of the waveguide modes, and details on FEM and FDTD simulations. The Supporting Information is available free of charge on the ACS Publications website at DOI: 10.1021/acs.nanolett.5b01135.

■ AUTHOR INFORMATION

Corresponding Authors

*E-mail a.d.v.dam@tue.nl.

*E-mail j.gomez@amolf.nl.

Notes

The authors declare no competing financial interest.

■ ACKNOWLEDGMENTS

This research is supported by the Dutch technology foundation STW, which is part of the "Netherlands Organisation for Scientific Research (NWO)", and partially funded by the Dutch Ministry of Economic Affairs. This work is also part of the research program of the "Foundation for Fundamental Research on Matter (FOM)", which is also financially supported by the NWO and is part of an industrial partnership program between Philips and FOM. The authors acknowledge the Spanish "Ministerio de Economía y Competitividad" for financial support through the Consolider-Ingenio project EMET (CSD2008-00066), and NANOPLAS+ (FIS2012-31070).

■ REFERENCES

(1) Wierer, J. J.; David, A.; Megens, M. M. *Nat. Photonics* **2009**, *3*, 163−169.

(2) Lundskog, A.; Hsu, C.-W.; Fredrik Karlsson, K.; Amloy, S.; Nilsson, D.; Forsberg, U.; Olof Holtz, P.; Janzén, E. *Light: Sci. Appl.* **2014**, *3*, e139.

(3) Svensson, C. P. T.; Mårtensson, T.; Trägårdh, J.; Larsson, C.; Rask, M.; Hessman, D.; Samuelson, L.; Ohlsson, J. *Nanotechnology* **2008**, *19*, 305201.

(4) Matioli, E.; Brinkley, S.; Kelchner, K. M.; Hu, Y.-L.; Nakamura, S.; DenBaars, S.; Speck, J. S.; Weisbuch, C. *Light: Sci. Appl.* **2012**, *1*, e22.

(5) Huang, M. H.; Mao, S.; Feick, H.; Yan, H.; Wu, Y.; Kind, H.; Weber, E.; Russo, R.; Yang, P. *Science* **2001**, *292*, 1897−9.

(6) Röder, R.; Ploss, D.; Kriesch, A.; Buschlinger, R.; Geburt, S.; Peschel, U.; Ronning, C. *J. Phys. D: Appl. Phys.* **2014**, *47*, 394012.

(7) Friedler, I.; Sauvan, C.; Hugonin, J. P.; Lalanne, P.; Claudon, J.; Gérard, J.-M. *Opt. Express* **2009**, *17*, 2095−110.

(8) Claudon, J.; Bleuse, J.; Malik, N. S.; Bazin, M.; Jaffrennou, P.; Gregersen, N.; Sauvan, C.; Lalanne, P.; Gérard, J.-M. *Nat. Photonics* **2010**, *4*, 174−177.

(9) Curto, A. G.; Volpe, G.; Taminiau, T. H.; Kreuzer, M. P.; Quidant, R.; van Hulst, N. F. *Science* **2010**, *329*, 930−3.

(10) Lee, K. G.; Chen, X. W.; Eghlidi, H.; Kukura, P.; Lettow, R.; Renn, A.; Sandoghdar, V.; Götzinger, S. *Nat. Photonics* **2011**, *5*, 166−169.

(11) Yan, R.; Gargas, D.; Yang, P. *Nat. Photonics* **2009**, *3*, 569−576.

(12) Maslov, A. V.; Ning, C. Z. *Opt. Lett.* **2004**, *29*, 572−574.

(13) Maslov, A. V.; Bakunov, M. I.; Ning, C. Z. *J. Appl. Phys.* **2006**, *99*, 024314.

(14) Diedenhofen, S. L.; Janssen, O. T. A.; Hocevar, M.; Pierret, A.; Bakkers, E. P. A. M.; Urbach, H. P.; Gómez Rivas, J. *ACS Nano* **2011**, *5*, 5830−5837.

(15) Grzela, G.; Paniagua-Domínguez, R.; Barten, T.; Fontana, Y.; Sánchez-Gil, J. A.; Gómez Rivas, J. *Nano Lett.* **2012**, *12*, 5481−5486.

(16) Chen, G.; Wu, J.; Lu, Q.; Gutierrez, H. R.; Xiong, Q.; Pellen, M. E.; Petko, J. S.; Werner, D. H.; Eklund, P. C. *Nano Lett.* **2008**, *8*, 1341−1346.

(17) Paniagua-Domínguez, R.; Grzela, G.; Gómez Rivas, J.; Sánchez-Gil, J. A. *Nanoscale* **2013**, *5*, 10582−90.

(18) Anderson, P. D.; Lin, C.; Povinelli, M. L. *Appl. Phys. A: Mater. Sci. Process.* **2014**, *117*, 1879−1884.

(19) Fontana, Y.; Grzela, G.; Bakkers, E. P. A. M.; Gómez Rivas, J. *Phys. Rev. B* **2012**, *86*, 245303.

(20) Wang, J.; Gudiksen, M. S.; Duan, X.; Cui, Y.; Lieber, C. M. *Science* **2001**, *293*, 1455−7.

(21) Mishra, A.; Titova, L. V.; Hoang, T. B.; Jackson, H. E.; Smith, L. M.; Yarrison-Rice, J. M.; Kim, Y.; Joyce, H. J.; Gao, Q.; Tan, H. H.; Jagadish, C. *Appl. Phys. Lett.* **2007**, *91*, 263104.

(22) van Weert, M. H. M.; Akopian, N.; Kelkensberg, F.; Perinetti, U.; van Kouwen, M. P.; Gómez Rivas, J.; Borgström, M. T.; Algra, R. E.; Verheijen, M. A.; Bakkers, E. P. A. M.; Kouwenhoven, L. P.; Zwiller, V. *Small* **2009**, *5*, 2134−2138.

(23) Grzela, G. Directional light emission and absorption by semiconductor nanowires. Ph.D. Thesis, Eindhoven University of Technology, 2013.

(24) Henneghien, A.-L.; Gayral, B.; Désières, Y.; Gérard, J.-M. *J. Opt. Soc. Am. B* **2009**, *26*, 2396.

(25) Ruda, H. E.; Shik, A. *J. Appl. Phys.* **2006**, *100*, 024314.

(26) Chen, H.-Y.; Yang, Y.-C.; Lin, H.-W.; Chang, S.-C.; Gwo, S. *Opt. Express* **2008**, *16*, 13465−75.

(27) Spirkoska, D.; Efros, A. L.; Lambrecht, W. R. L.; Cheiwchanchamnangij, T.; Fontcuberta i Morral, A.; Abstreiter, G. *Phys. Rev. B* **2012**, *85*, 045309.
(28) Birman, J. *Phys. Rev.* **1959**, *114*, 1490−1492.
(29) Wilhelm, C.; Larrue, A.; Dai, X.; Migas, D.; Soci, C. *Nanoscale* **2012**, *4*, 1446−54.
(30) Paniagua-Domínguez, R.; Grzela, G.; Gómez Rivas, J.; Sánchez-Gil, J. A. *Proc. SPIE* **2013**, *8808*, 88080J.
(31) Joannopoulos, J. D.; Johnson, S. G.; Winn, J. N.; Meade, R. D. *Photonic Crystals: Molding the Flow of Light*, 2nd ed.; Princeton University Press: Princeton, NJ, 2008.
(32) Gregersen, N.; Nielsen, T. R.; Claudon, J.; Gérard, J.-M.; Mø rk, J. *Opt. Lett.* **2008**, *33*, 1693−1695.
(33) Reimer, M. E.; Bulgarini, G.; Akopian, N.; Hocevar, M.; Bouwes Bavinck, M.; Verheijen, M. A.; Bakkers, E. P. A. M.; Kouwenhoven, L. P.; Zwiller, V. *Nat. Commun.* **2012**, *3*, 737.
(34) Bulgarini, G.; Reimer, M. E.; Zehender, T.; Hocevar, M.; Bakkers, E. P. A. M.; Kouwenhoven, L. P.; Zwiller, V. *Appl. Phys. Lett.* **2012**, *100*, 121106.
(35) Mattila, M.; Hakkarainen, T.; Mulot, M.; Lipsanen, H. *Nanotechnology* **2006**, *17*, 1580−1583.